Energy and angular distributions of detached electrons in a solvable model of ion-atom collisions

J. H. Macek and S. Yu. Ovchinnikov*
Department of Physics and Astronomy, University of Tennessee, Knoxville, Tennessee 37996-1501
and Oak Ridge National Laboratory, P.O. Box 2008, Oak Ridge, Tennessee 37831

E. A. Solov'ev
Macedonian Academy of Sciences and Arts, Research Center for Energy and Informatics, P.O. Box 428, 91000 Skopje, Macedonia
(Received 29 October 1998)

Electron energy and angular distributions are computed for a model of atom–negative-ion collisions. In this model, electron-atom interactions are represented by zero-range potentials in an approximation where two identical atoms move along straight-line classical trajectories in head-on collisions. Analytic expressions for the ionization amplitudes are interpreted in terms of Sturmian eigenvalues and eigenfunctions. At high velocity, the computed distributions exhibit direct excitation and continuum capture cusps in addition to the binary encounter ridge. At low velocities, a single feature corresponding to an electron distribution centered midway between the target and projectile emerges. For initial conditions corresponding to gerade symmetry a single broad peak appears, while for ungerade symmetry there is a node at the midpoint so that the peak splits into two parts. It is confirmed that the advanced adiabatic approximation gives an accurate description of the ungerade distribution at low and intermediate velocities. [S1050-2947(99)05408-6]

PACS number(s): 34.80.Dp, 34.20.Mq, 34.10.+x, 34.50.Fa

I. INTRODUCTION

Electron energy and angular distributions have long been used to probe the dynamics of ion-atom collisions. At high energy, where Born-type approximations are applicable, fairly complete theories of single-electron ionization have emerged [1]. Three features dominate the spectrum in this region, namely, the binary encounter peak, the continuum capture cusp, and the direct ionization cusp. The binary encounter peak occurs for all systems and the cusps are characteristic of the Coulomb interaction which produces a $1/k$ singularity in the Galilean invariant cross section [2]. All three features are described quantitatively by the continuum distorted-wave–eikonal initial state theory, for example [3,4]. This and related theories associate a specific mechanism with a specific physical feature. The binary encounter ridge is associated with quasifree scattering of projectiles with target atoms and the continuum capture cusp with a transfer of electrons from the target to unbound states of the projectile.

Alternatively, the situation is much less clear at low velocity. Four mechanisms for ionization have been identified, namely, the top-of-barrier mechanism [5–7], the superpromotion mechanism [8], a ''radial decoupling'' mechanism analogous to the well-known ''rotational coupling'' mechanism [9], and real promotion to the continuum [10]. The latter process occurs only for multielectron systems such as negative-ion collisions with neutral atoms. A complete theory of the top-of-barrier distribution has been developed [11], the advanced adiabatic theory has given expressions for the fast electron portion of the superpromotion and real promotion distributions [10], and there is no theory of the radial decoupling electron distribution. Models of ionization at low energies when an adiabatic level is promoted through a series of avoided crossings have been solved [12,13]. These models show that ionization occurs at low velocity and have served to guide later developments.

Because of the lack of a generally valid theory, it is not possible to associate a specific feature of the electron distribution with a specific mechanism. Although there have been many attempts to do this for the top-of-barrier mechanism, no real consensus has emerged. Finally, none of these theories are able to connect with high-velocity distributions. Rather, the advanced adiabatic theory employs approximate solutions in the limit $v \to 0$ while the high-velocity theories employ approximate solutions in the opposite limit $1/v \to 0$, but no universal expression holds at all velocities. There have also been attempts at exact *ab initio* simulations of the electron distributions, but these are still in the development stage [14].

In order to make progress in this area, we consider a nontrivial model of ion-atom collisions, namely, the two zero-range potential (ZRP) model at zero impact parameter where the atomic species move along classical trajectories $R(t)$. This model has been solved exactly in both one and three dimensions [15–18] hence it gives a universal amplitude valid for all v. The corresponding electron distributions for low impact velocities have been given in the literature, however, the distributions at high velocities have not. The purpose of this manuscript is to study the high-velocity distributions for this model and to examine their connection with the low-energy features. While it is highly simplified and lacks both super-promotion and top-of-barrier mechanisms, the model does predict ionization at low energy. As we will show, it exhibits the three high-energy features known from ion-atom collisions. It also exhibits features at low energy that will be discussed in terms of the advanced adiabatic theory. Finally, the steps used to solve the exact model closely parallel those used in the Sturmian [19] and

*Permanent address: Ioffe Physical Technical Institute, St. Petersburg, Russia.

advanced adiabatic [10] formulations of ion-atom collisions. This theory enables one to see how adiabatic eigenstates, generally considered appropriate at low relative ion velocity, also describe high-velocity features.

Transformation to an accelerated reference frame where both the target and projectile are stationary is a first step in formulating a Galilean invariant theory of ion-atom collisions [20], and is a key step in solving the ZRP model [17]. The ZRP model provides a valuable illustration of this transformation. Most important for the theory of electron distributions is the appearance of a factor $\exp[-ir^2\dot{R}(t)/2R(t)]$ that is common to both the general theory of ion-atom collisions and the exact solution of the ZRP. Conventional approaches typically omit such a factor, thus it is useful to show an exact solution where it is known to occur. The transformation to the accelerated frame employs the scaled electron coordinate $\mathbf{q}=\mathbf{r}/R(t)$ and a ''scaled'' time $d\tau = dt/R(r)^2$. This representation has been extensively discussed in the literature thus it will be taken as the starting point for the analysis presented here.

It is possible to interpret the exact solution of the ZRP model in terms of a Sturmian function [21] of the type used in the outgoing wave Sturmian theory of ion-atom collisions [20]. For general ion-atom collisions an infinite set of Sturmian functions represent an alternative to the more standard Born-Oppenheimer adiabatic basis set. In contrast to the adiabatic set, the Sturmian set naturally incorporates ionization channels [19]. Indeed, the ZRP model has only one Sturmian function yet it describes ionization. We show that the exact solution can be written in terms of one Sturmian eigenvalue and the associated Sturmian function. The wave function in the ZRP model therefore has the same form as the one-Sturmian approximation for proton–hydrogen-atom collisions. For this reason the ZRP model provides a useful test of approximate solutions relevant to ion-atom collisions. In this connection it has been noted that another widely used nontrivial model, the Demkov-Osherov [13] multicrossing model, is also solved in terms of one Sturmian function [22].

With an exact solution it is possible to study the connection between low- and high-velocity features. We find that the binary encounter peak disappears at low velocity while the direct and continuum capture peaks centered at electron velocities $\mathbf{k}=\mathbf{v}_T$ and $\mathbf{k}=\mathbf{v}_P$, where $\mathbf{v}_T$ and $\mathbf{v}_P$ are target and projectile velocities, respectively, merge to form one peak centered midway between target and projectile at low relative velocity. This is most noticeable for the gerade (g) symmetry. For the ungerade (u) symmetry, there must be a node at the midpoint, thus this distribution shows two peaks well separated from each other and not associated with the target and projectile.

An interesting feature emerges when comparing distributions at high and low velocity. One can compute electron distributions for initial conditions corresponding to the electron localized around the target T, or localized around the projectile P. We call these initial conditions ''atomic'' initial conditions. Alternatively, one can compute electron distributions corresponding to either g or u symmetries. We call these initial conditions ''molecular'' initial conditions. At high velocities the ''atomic'' initial conditions give smooth distributions showing only target, projectile, and binary encounter peaks. Distributions corresponding to ''molecular'' initial conditions employ coherent superpositions of the ''atomic'' amplitudes. These superpositions of smooth amplitudes produce oscillating distributions owing to interference. Thus, at high velocities the distributions are smooth in the atomic representation, but show interference effects in the molecular representation.

The situation is exactly reversed at low ion velocities. Here the molecular states of g and u symmetry separate dynamically. In this case the electron distributions are smooth for molecular initial conditions but show interference oscillations for atomic initial conditions. We will show that these interference effects give rise to the classical Fermi acceleration peaks [18]. At intermediate velocities, not reported here, where the target and projectile peaks just begin to separate no initial conditions are preferred and interference effects appear for all initial conditions.

It is not known if these features persist for real ion-atom collisions, however, it would appear that the qualitative features should be present. Atomic initial conditions certainly give smooth distributions in the high-velocity CDW-EIS approximation, while molecular initial conditions should show interference effects owing to rapidly varying phase factors. A complete theory for low velocities has not yet emerged, although the interference oscillations have been computed for the top-of-barrier electrons. It has been proposed that such interference is the origin of some oscillations observed experimentally. Alternatively, with molecular initial conditions, interference between g and u amplitudes is absent.

Expressions for low-velocity electron distributions have been derived in the advanced adiabatic approximation [10]. These analytic expressions are compared with the exact distributions. At low ion velocities, the approximate expressions reproduce the exact distributions fairly well for all electron velocities in the case of u initial conditions, but fail for the g initial conditions. An alternative approximate distribution is derived for the g case by expanding the Sturmian eigenvalue about its first zero. The approximate Sturmian g distribution agrees well with the exact distributions in the low-velocity limit.

The plan of the manuscript is as follows. The exact solutions of the ZRP models are reviewed in Sec. II and the solutions are interpreted in terms of the Sturmian theory of ion-atom collisions. In Sec. III, the exact solutions are used to compute electron distributions at high, low, and intermediate electron velocities. The oscillatory structure of the distributions is noted and discussed. Section IV discusses the distributions given by the advanced adiabatic approximation. This approximation is found to be quite accurate for the u boundary conditions. Essentially, if the adiabatic potential curve enters the continuum at nonzero, positive values of R, the formulas of the advanced adiabatic approximation are quite accurate at low velocity. This happens for the u symmetry but for the g symmetry, promotion occurs at negative values of R. In this case, the advanced adiabatic approximation fails, but an alternative, closely related, formula works fairly well. Finally, the distributions at high velocity are shown to follow from an expansion of the Sturmian eigenvalue about its first zero. Approximate expressions in good agreement with the computed cross sections are obtained.

II. REVIEW OF STURMIAN THEORY FOR TWO ZERO-RANGE POTENTIALS

We consider two identical ZRPs ($Z_1=Z_2=Z/2$) characterized by the binding energy $E=-Z_1^2/2$ of an attached electron. The ZRPs follow classical straight-line trajectories. The Schrödinger equation for this system in scaled coordinates is [17,23]

$$\left[i\frac{\partial}{\partial\tau}-H_0(\mathbf{q})\right]\varphi(\tau,\mathbf{q})=0, \tag{2.1}$$

where

$$H_0(\mathbf{q})=-\frac{1}{2}\nabla_{\mathbf{q}}^2+V_0(\mathbf{q}). \tag{2.2}$$

In the scaled space the Galilean invariant solution is related to the solution of the time-dependent Schrödinger equation in the usual space by the transformation [23], $\Psi(t,\mathbf{r})=R^{-3/2}\exp[(ir^2/2R)(dR/dt)]\varphi(\tau,\mathbf{q})$. The function $\varphi(\tau,\mathbf{q})$ satisfies the following boundary conditions at the ZRPs:

$$\frac{\partial[\varphi(\tau,\mathbf{q})|\mathbf{q}\pm\hat{\mathbf{z}}/2|]}{\partial q}-Z_1\tilde{R}(\tau)[\varphi(\tau,\mathbf{q})|\mathbf{q}\pm\hat{\mathbf{z}}/2|]\Big|_{|\mathbf{q}\mp\hat{\mathbf{z}}/2|=0}=0, \tag{2.3}$$

where

$$\tilde{R}(\tau)=-\frac{1}{\nu\tau},\quad -\infty<\tau\leqslant 0. \tag{2.4}$$

The boundary conditions specify the ZRPs, while the additional potential $V_0(\mathbf{q})$ has been included for generality. This potential is usually absent for head-on collisions, but includes rotational coupling and harmonic oscillator terms at nonzero impact parameters [23]. Even for head-on collisions it is instructive to retain the $\mathbf{q}$-dependent potential even though such a potential has no immediate physical significance. For future reference it should be noted that plane waves in $(\mathbf{r},t)$ space are proportional to Feynman's propagator in $(\mathbf{q},\tau)$ space.

Wave functions and ionization amplitudes for the model with $V_0(\mathbf{q})=0$ have been obtained earlier [15,17]. Here we will interpret these quantities in terms of the Sturmian eigenvalues and eigenfunctions of the model.

Sturmian functions are solutions of the equation

$$[H_0(\mathbf{q})-\omega]S_\nu(\omega;\mathbf{q})=0, \tag{2.5}$$

with outgoing wave boundary conditions

$$\frac{\partial S_\nu(\omega;\mathbf{q})}{\partial q}-i\sqrt{2\omega}S_\nu(\omega;\mathbf{q})\to 0\ \text{ as }\ q\to\infty \tag{2.6}$$

and with boundary conditions at the ZRPs

$$\frac{\partial[S_\nu(\omega;\mathbf{q})|\mathbf{q}\pm\hat{\mathbf{z}}/2|]}{\partial q}-Z_1\rho_\nu(\omega)[S_\nu(\omega;\mathbf{q})|\mathbf{q}\pm\hat{\mathbf{z}}/2|]\Big|_{|\mathbf{q}\mp\hat{\mathbf{z}}/2|=0}=0, \tag{2.7}$$

where $\rho_\nu(\omega)$ is the Sturmian eigenvalue. Notice that $\rho_\nu(\omega)$ multiplies the strength Z_1 of the potential. Since the eigenvalue is the coefficient of the potential, we follow the standard usage in the physics literature and refer to $\rho_\nu(\omega)$ as the Sturmian eigenvalue.

There are only two Sturmian functions for two ZRPs. For identical ZRPs the functions have gerade and ungerade symmetry so that $\nu=\pm$. The Sturmian functions are

$$S_\pm(\omega;\mathbf{q})=2\sqrt{\frac{\pi}{Z_1}}G_\pm(\omega;\mathbf{q},\hat{\mathbf{z}}/2), \tag{2.8}$$

where

$$G_\pm(\omega;\mathbf{q},\mathbf{q}')=\frac{1}{2}[G(\omega;\mathbf{q},\mathbf{q}')\pm G(\omega;\mathbf{q},-\mathbf{q}')]. \tag{2.9}$$

In these expressions, $(+)$ is used for the gerade state, $(-)$ for the ungerade state, and $G(\omega;\mathbf{q},\mathbf{q}')$ is the Green function for H_0. The corresponding Sturmian eigenvalues are

$$\rho_\pm(\omega)=-\frac{1}{Z_1}\lim_{\mathbf{q}\to\hat{\mathbf{z}}/2}\left[2\sqrt{\pi Z_1}S_\pm(\omega;\mathbf{q})-\frac{1}{|\mathbf{q}-\hat{\mathbf{z}}/2|}\right]. \tag{2.10}$$

We normalize the Sturmians according to the usual condition [21]

$$\int S_\nu(\omega;\mathbf{q})S_\nu(\omega;\mathbf{q})d^3\mathbf{q}=-\frac{d\rho_\nu(\omega)}{d\omega}. \tag{2.11}$$

The Sturmian basis relates closely to the more familiar adiabatic basis, which obtains when $\rho_\nu(\omega)$ is replaced by the coordinate R and Eq. (2.10) is solved for $\omega(R)$. Then the adiabatic energy eigenvalues $E_\nu(R)$ are given by

$$E_\nu(R)=\frac{\omega_\nu(R)}{R^2}. \tag{2.12}$$

At the physical values $\rho_\nu(\omega)=R$ the Sturmians are equal to the adiabatic eigenfunctions up to an overall normalization constant. In effect, the adiabatic eigenvalues are obtained from the function $\omega(\rho)$ inverse to $\rho(\omega)$. Because the inverse function may have many branches it is possible to have many adiabatic eigenvalues $E(R)$ for real R. This is why one Sturmian may suffice to write the exact solution, whereas an infinite number of adiabatic basis functions are needed for the same purpose.

When the function $G(\omega;\mathbf{q},\mathbf{q}')$ is the free-particle Green function

$$G(\omega;\mathbf{q},\mathbf{q}')=\frac{1}{2\pi}\frac{\exp(i\sqrt{2\omega}|\mathbf{q}-\mathbf{q}'|)}{|\mathbf{q}-\mathbf{q}'|}, \tag{2.13}$$

the Sturmian eigenvalues $\rho_\pm(\omega)$ can be written explicitly as

$$\rho_\pm(\omega)=-\frac{1}{Z_1}[i\sqrt{2\omega}\pm\exp(i\sqrt{2\omega})]. \tag{2.14}$$

This set of Sturmian functions is used to compute the energy and angular distributions reported in Sec. IV.

Since the states of different symmetry do not interact, we can consider separately the solutions of Eq. (2.1) with different symmetry. We seek solutions using the Fourier transform

$$\varphi(\tau,\mathbf{q})=\frac{1}{\sqrt{-2\pi i}}\int_{-\infty}^{\infty}d\omega\,\exp(-i\omega\tau)\chi(\omega,\mathbf{q}), \tag{2.15}$$

where $\chi(\omega,\mathbf{q})$ satisfies the equation

$$[H_0(\mathbf{q})-\omega]\chi(\omega,\mathbf{q})=0 \tag{2.16}$$

and boundary conditions at the ZRPs

$$i\frac{\partial}{\partial\omega}\left\{\frac{\partial}{\partial q}[\chi(\omega,\mathbf{q})|\mathbf{q}\pm\hat{\mathbf{z}}/2|]\right\} -\frac{Z_1}{\nu}[\chi(\omega,\mathbf{q})|\mathbf{q}\pm\hat{\mathbf{z}}/2|]\Big|_{|\mathbf{q}\mp\hat{\mathbf{z}}/2|=0}=0. \tag{2.17}$$

The wave function $\chi_i(\omega,\mathbf{q})$ that corresponds to the initial bound state continuum state is written in the form

$$\chi_i(\omega,\mathbf{q})=S_\nu(\omega;\mathbf{q})B^i_\nu(\omega) \tag{2.18}$$

and the wave function $\chi_{\mathbf{k}}(\omega,\mathbf{q})$ that corresponds to the final continuum state in the form

$$\chi_{\mathbf{k}}(\omega,\mathbf{q})=\frac{1}{\sqrt{2\pi}\nu^{3/2}}G_\nu(\omega;\mathbf{k}/\nu,\mathbf{q})+S_\nu(\omega;\mathbf{q})B^{\mathbf{k}}_\nu(\omega), \tag{2.19}$$

where $\nu=\pm$.

Using Eqs. (2.17) and (2.7) one easily finds equations for the coefficients $B^i_\nu(\omega)$ and $B^{\mathbf{k}}_\nu(\omega)$:

$$i\frac{\partial}{\partial\omega}[B^i_\nu(\omega)\rho_\nu(\omega)]+\frac{1}{\nu}B^i_\nu(\omega)=0 \tag{2.20}$$

and

$$i\frac{\partial}{\partial\omega}[B^{\mathbf{k}}_\nu(\omega)\rho_\nu(\omega)]+\frac{1}{\nu}B^{\mathbf{k}}_\nu(\omega)=-\frac{1}{\sqrt{2\pi}\nu^{3/2}}\frac{\partial S_\nu(\omega,\mathbf{k}/\nu)}{\partial\omega}. \tag{2.21}$$

The solutions of these equations are

$$B^i_\nu(\omega)=\frac{1}{\sqrt{\nu}}\frac{D_\nu(\omega)}{\rho_\nu(\omega)}\delta_{\nu i} \tag{2.22}$$

and

$$B^{\mathbf{k}}_\nu(\omega)=\frac{1}{\sqrt{2\pi}\nu^{3/2}}\frac{D_\nu(\omega)}{\rho_\nu(\omega)}\int_{-\infty}^{\omega}d\omega'\frac{\partial S_\nu(\omega',\mathbf{k}/\nu)}{\partial\omega'}D_\nu^{-1}(\omega'), \tag{2.23}$$

where

$$D_\nu(\omega)=\exp\left[\frac{i}{\nu}\int_0^\omega\frac{d\omega'}{\rho_\nu(\omega')}\right]. \tag{2.24}$$

The integration constants have been chosen so that the set $\varphi_i(\tau,\mathbf{q})$, $\varphi_{\mathbf{k}}(\tau,\mathbf{q})$ is orthonormal.

The transition amplitudes to the continuum are given by the standard formula

$$T_{\mathbf{k},i}=\int\varphi_i^{\rm out}(\tau,\mathbf{q})\varphi_{\mathbf{k}}^{\rm in}(\tau,\mathbf{q})d^3\mathbf{q} =\frac{i}{2\pi}\int_{-\infty}^{\infty}d\omega\int_{-\infty}^{\infty}d\omega' e^{-i(\omega-\omega')\tau} \times\int\chi_i^{\rm out}(\omega',\mathbf{q})\chi_{\mathbf{k}}^{\rm in}(\omega,\mathbf{q})d^3\mathbf{q}. \tag{2.25}$$

This expression is computed explicitly in terms of Sturmian eigenvalues and eigenfunctions in Appendix A. There we obtain

$$T_{\mathbf{k},i}=\frac{i}{\sqrt{2\pi\nu}}\int_0^\infty d\omega\left\{\frac{\partial S_\nu(\omega;\mathbf{k}/\nu)}{\partial\omega}D_\nu(\omega)[1-T_\nu(\omega)] -\frac{\partial S^*_\nu(\omega;\mathbf{k}/\nu)}{\partial\omega}[D_\nu(\omega)-T_\nu(0)D^*_\nu(\omega)]\right\}, \tag{2.26}$$

where

$$T_\nu(\omega)=-\frac{i}{\nu}\frac{1}{D^2_\nu(\omega)}\int_\omega^\infty d\omega'\frac{\rho_\nu(\omega')-\rho^*_\nu(\omega')}{\rho^2_\nu(\omega')}D^2_\nu(\omega'). \tag{2.27}$$

Equation (2.26) is the main result of this section. It is easy to evaluate numerically since it expresses the transition amplitude in terms of Sturiman eigenvalues and eigenfunctions at real ω. These quantities are connected to the more familiar adiabatic eigenvalues and eigenfunctions through Eq. (2.12). Using this connection formula it is possible to change variables from ω to ρ in Eq. (2.26), provided the adiabatic function is interpreted in the sense articulated by Demkov [24].

With this change of variables three features emerge. First, $D_\nu^{-1}(\omega)$ is found to be proportional to the adiabatic phase factor $\exp[-(i/\nu)\int_{\rho(0)}^{\rho}E_\nu(\rho')d\rho']$. Secondly the Sturmian function is replaced by the adiabatic function. Finally, the limits of integration are $\rho(0)$ and $\rho(\omega)$. In general, both limits are complex, thus the ionization amplitude is then expressed as an integral along some contour in the complex ρ plane of an integrand involving the adiabatic function $\Phi(R;\mathbf{q})$ and the adiabatic phase factor. This shows that adiabatic functions and eigenvalues are relevant even at high velocity provided these quantities are taken at complex values of the coordinate $\rho=R$, and provided the adiabatic wave functions are expressed in scaled coordinates. In this sense, adiabatic functions are universally applicable even in the absence of a small mass ratio or other such adiabatic parameter. Furthermore, these functions enter into the theory in much the same way that they do in the hidden crossing theory, namely, their values at complex R are used to compute transitions between states.

The electron distributions are given in the Galilean invariant form

$$\frac{d^3P}{dk^3}=|T_{\mathbf{k},\mathrm{i}}|^2. \tag{2.28}$$

Integrating Eq. (2.28) over all impact parameters would give the Galilean invariant cross section. Because we are working only at an impact parameter equal to zero, we quote only the differential probability. The total ionization probability P_{ion} at zero impact parameter is obtained by integrating Eq. (2.28) over all electron momenta. Alternatively, unitarity gives

$$P_{\mathrm{ion}}=1-|T_{\nu}(0)|^2. \tag{2.29}$$

This equation has been used to check the numerical calculations reported in Sec. III.

Amplitudes for $V_0(\mathbf{q})=0$

When $V_0(\mathbf{q})=0$ the Sturmian eigenvalues are

$$\rho^{\pm}(p)=-\frac{2}{Z}[ip\pm\exp(ip)], \tag{2.30}$$

where $p=\sqrt{2\omega}$. The electron distributions with molecular initial conditions are given by

$$T^{\pm}_{\mathbf{k},i}=\frac{i}{2v\pi\sqrt{Z}}\left[F^{\pm}\left(\left|\frac{\mathbf{k}}{v}+\frac{\hat{\mathbf{v}}}{2}\right|\right)\pm F^{\pm}\left(\left|\frac{\mathbf{k}}{v}-\frac{\hat{\mathbf{v}}}{2}\right|\right)\right], \tag{2.31}$$

where

$$\begin{aligned}F^{\pm}(k)=&\int_0^{\infty}dp\,\exp(ikp)\exp\left[-\frac{y^{\pm}(p)}{2}\right]\{1-T^{\pm}(p)\}\\&+\int_0^{\infty}dp\,\exp(-ikp)\left\{\exp\left[-\frac{y^{\pm}(p)}{2}\right]\right.\\&\left.-T^{\pm}(0)\exp\left[-\frac{[y^{\pm}(p)]^*}{2}\right]\right\},\end{aligned} \tag{2.32}$$

$$y^{\pm}(p)=-i\frac{2}{v}\int_0^p\frac{p'dp'}{\rho^{\pm}(p')}, \tag{2.33}$$

$$\begin{aligned}T^{\pm}(x)=&-\frac{i}{v}\exp[y^{\pm}(x)]\int_x^{\infty}dpp\,\frac{\rho^{\pm}(p)-[\rho^{\pm}(p)]^*}{[\rho^{\pm}(p)]^2}\\&\times\exp[-y^{\pm}(p)].\end{aligned} \tag{2.34}$$

The subscript i is redundant since the molecular symmetry is denoted by the $\pm$ superscript, but because linear combinations of the $\pm$ amplitudes are used to obtain atomic initial conditions, it is useful to retain the redundant subscript i.

For the two one-dimensional (1D) ZRP model the same formulas (2.31)–(2.34) apply except that $[\rho^{\pm}(p)]^2$ in the denominator of Eq. (2.34) is replaced by $-|\rho^{\pm}(p)|^2$, and the normalization factor in Eq. (2.31) is $(i/2)\sqrt{Z/2\pi}$. In both cases the lower limit $\rho(0)$ is real but not zero, while $\rho(\infty)$ is infinite and complex. Thus a contour of integration in the complex R plane, discussed in the preceding section, starts out on the real axis but must go into the complex plane to reach the upper limit. Note that for the g state, the contour starts at negative values of ρ, which naturally cannot be identified with physical values of R.

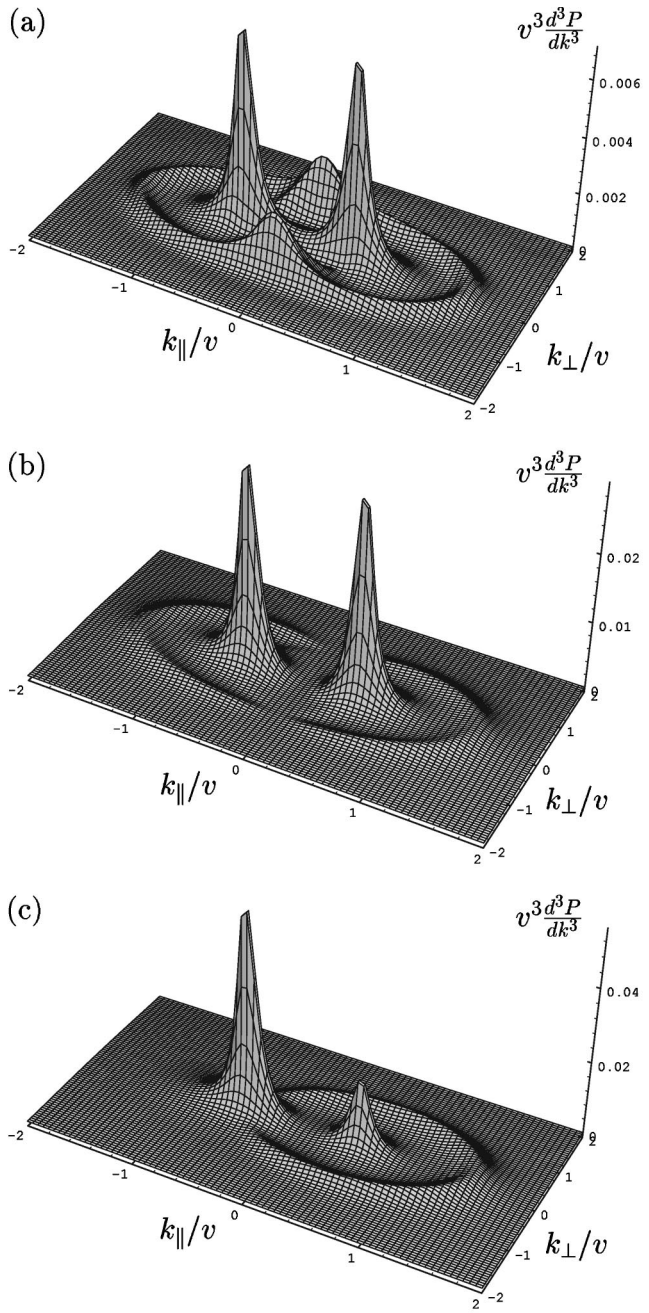

FIG. 1. Electron distributions $v^3\,d^3P/dk^3$ vs k/v for $v=10$ a.u. Distributions corresponding to (a) ''gerade'' and (b) ''ungerade'' symmetry and (c) the distribution corresponding to an electron initially on the projectile are shown.

III. ELECTRON DISTRIBUTIONS

A. Distribution for high velocity

The electron distributions corresponding to g and u states at a relatively high velocity of $v=10$ are shown in Figs. 1(a) and 1(b). In both cases there are two peaks, one centered at the target and one at the projectile. The two peaks are well separated from an oval-shaped ridge.

The ridge is seen more clearly in Fig. 1(c) where the distribution corresponding to ''atomic'' initial conditions, where the electron is attached to the projectile, is shown. Again, there is a prominent peak centered at $\mathbf{k}=\mathbf{0}$ corresponding to slow electrons in the target frame, a smaller peak centered at $\mathbf{k}=\mathbf{1}$ corresponding to slow electrons in the projectile frame, and the binary encounter ridge at $|\mathbf{k}-\mathbf{v}|=v$. These features are similar to those observed in high-energy ion-atom collisions.

Since these features are well understood in terms of high-velocity approximations we anticipate that these features will emerge if the exact formulas of Sec. III are expanded in powers of $1/v$ and only the lowest nonvanishing terms retained. The details of this calculation are given in Appendix B, where we obtain for the function $F^{\pm}(k)$ the result

$$F^{\pm}(k)\approx\frac{2Z_1}{v}\frac{z^{\pm}}{Z_1/v+ik}\pm\frac{2Z_1^2}{v^2}\left\{\frac{2-(k+1)[\mathrm{Im}\,x^{\pm}(0)-2]}{[(Z_1/v)^2+(k+1)^2]^{1/2}}-\frac{2-(k-1)[\mathrm{Im}\,x^{\pm}(0)+2]}{[(Z_1/v)^2+(k-1)^2]^{1/2}}\right\},\tag{3.1}$$

where $x^{\pm}(0)$ and $z^{\pm}$ are constants. Their numerical values are $x^{+}(0)=-1.13-i0.13$, $z^{+}=0.65+i0.38$, $x^{-}(0)=-i0.76$, $z^{-}=1.56-i0.52$, and $\beta=1$.

The function $F^{\pm}(k')$ peaks at $k'=0$ and $k'=1$. Recalling that the transition amplitude $T_{\mathbf{k}}^{\pm}$ with molecular initial conditions corresponds to a superposition of two terms, one with $k'=|\mathbf{k}-\mathbf{v}/2|$ and one with $k'=|\mathbf{k}+\mathbf{v}/2|$, we see that the peaks with $k'=|\mathbf{k}\pm\hat{\mathbf{v}}/2|=0$ correspond to electrons localized near the target and projectile, respectively. Similarly, the peak in $F^{\pm}(k')$ with $k'=1$ accounts for the oval-shaped ridge in Figs. 1(a) and 1(b).

Linear superpositions of the g and u molecular amplitudes form amplitudes corresponding to electrons on the target T or projectile P. Because the third term in $F^{\pm}$ becomes independent of the g and u symmetry when $k'=1$, the atomic transition amplitudes show a ridge centered at the velocity of P or T but not both. This ridge is readily recognized as the binary encounter ridge familiar from the theory of high-velocity collisions.

Alternatively, the coefficient of the first term on the right hand side of Eq. (3.1) depends explicitly upon the molecular symmetry. Both peaks corresponding to $k'=|\mathbf{k}-\mathbf{v}/2|/v$ and $k'=|\mathbf{k}+\mathbf{v}/2|/v$ therefore appear in Fig. 1(c), although with unequal magnitudes. The peak near $\mathbf{k}=\mathbf{v}$ corresponds to direct ionization of the projectile electron while the peak near $\mathbf{k}=\mathbf{0}$ corresponds to continuum electron capture. Both peaks have exactly the shape predicted by Garraboti and Barrachina [25] for electron transfer to continuum states of neutral projectiles, namely,

$$\sigma\propto\frac{1}{Z_1^2+|\mathbf{k}-\mathbf{v}|^2}.\tag{3.2}$$

From this analysis one sees that the ZRP model has all of the qualitative features of ion-atom and atom–negative-ion collisions in the high-velocity region. Furthermore, just one Sturmian function and eigenvalue $\rho(\omega)$ gives the exact electron distribution. This holds despite the fact that the Sturmian eigenfunction is just the ground state adiabatic eigenfunction taken at $R=\rho(\omega)$. This example shows that if the adiabatic functions are interpreted as Sturmian functions at appropriate values of R, which may be complex, they do describe high-velocity collisions.

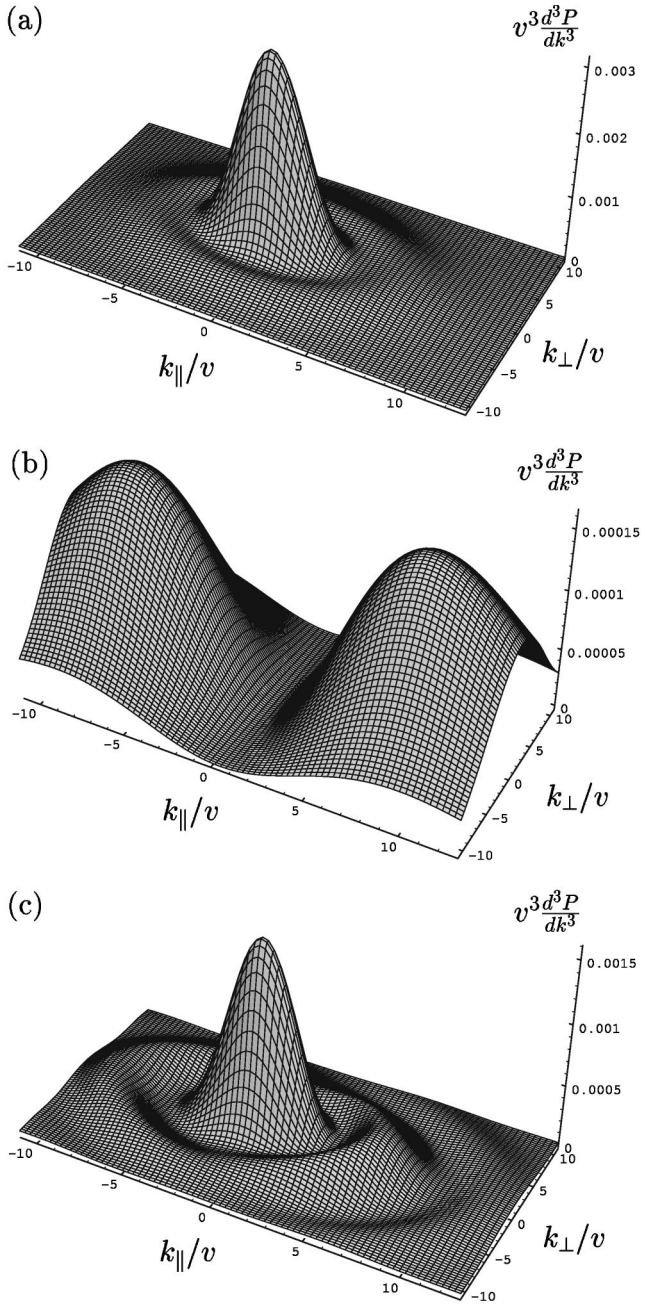

FIG. 2. Electron distributions $v^3\,d^3P/dk^3$ vs k/v for $v=0.1$ a.u. Distributions corresponding to (a) ''gerade'' and (b) ''ungerade'' symmetry and (c) the distribution corresponding to an electron initially in the projectile are shown. Out of phase oscillations correspond to Fermi acceleration.

B. Distributions for low velocity

The exact electron distributions corresponding to g and u states at low velocity $v\approx1$ are shown in Figs. 2(a) and 2(b). For g states, there is just one peak centered at $\mathbf{k}=\mathbf{v}/2$ and a small ridge at $k\approx7$ a.u. In comparison with the high-velocity distributions one notes that the binary encounter peak com-

pletely disappears and the separate T and P peaks merge into one peak centered between the target and projectile. The situation is similar for the ungerade state where now there is a node at the midpoint owing to symmetry requirements. In this case there is also no binary encounter peak, and the separate target and projectile peaks have merged into a peak with a node exactly midway between target and projectile. There is also no small ridge at high electron momentum.

Figure 2(c) shows the distribution with atomic initial conditions. This distribution exhibits the peak at the center of mass velocity seen in Fig. 1(a), but also shows a series of interference features. Because the g and u distributions are smooth, it is apparent that the oscillations in the atomic representation are due to interference between the g and u amplitudes. Furthermore, the oscillations in the forward and backward directions are out of phase since the peaks are at $(2n-1/2)v$ in the forward direction and at $(2n+1/2)v$ in the backward direction. Such peaks are attributed classically to Fermi acceleration where the electron bounces back and forth between the target and the projectile, picking up two units of velocity with each collision [18].

To describe the g and u distributions the integrals in Eq. (2.32) may be evaluated in the stationary phase approximation appropriate in the limit as $v\rightarrow 0$. For this purpose we introduce a new function $p_\nu(k)$ reciprocal to $k_\nu(p)=p/\rho_\nu(p)$. If $\mathrm{Im}\,p_\nu(k)<\mathrm{Re}\,p_\nu(k)$, then the integrals in Eq. (2.26) have stationary phase points $p=p_\nu(k)$ and we obtain

$$|T_{\mathbf{k},i}|^2\approx\frac{1}{v}\left|\frac{dp_\nu(k)}{dk}c_\nu^2(p_\nu(k),\hat{\mathbf{k}})\right|\exp\left[-\frac{2}{v}\,\mathrm{Im}\int_0^k p_\nu(k')dk'\right], \tag{3.3}$$

where $i=\nu$ and $c_\nu(p,\hat{\mathbf{k}})$ is defined by

$$S_\nu(p^2/2;\mathbf{q})\rightarrow c_\nu(p,\hat{\mathbf{q}})\frac{\exp(ipq)}{q}\quad\text{as}\quad q\rightarrow\infty. \tag{3.4}$$

Equation (3.3) is equivalent to advanced adiabatic approximation defined in Ref. [10]. In that fundamental paper the expression

$$|T_{\mathbf{k},i}|^2=\frac{1}{v}\left|\frac{dR_\nu(E)}{dE}C_\nu^2(E,\hat{\mathbf{k}})\right|\exp\left[-\frac{2}{v}\,\mathrm{Im}\int_0^E R(E')dE'\right] \tag{3.5}$$

was derived. Here $E=k^2/2$, $R(E)$ is the function reciprocal to $E(R)$, and $C_\nu(E,\hat{\mathbf{k}})$ is an angular part in the asymptotic limit of the electronic adiabatic wave function;

$$\Phi_\nu(R(E);\mathbf{r})\rightarrow C_\nu(E,\hat{\mathbf{r}})\frac{\exp(ikr)}{r}\quad\text{as}\quad r\rightarrow\infty. \tag{3.6}$$

The equivalence of the Sturmian and advanced adiabatic expressions follows from $R(E)=p(k)/k$ and the identities

$$\begin{aligned}c_\nu(p(k),\hat{\mathbf{k}})&=R(E)^{1/2}\left(\frac{dR}{p\,dp}\right)^{1/2}C_\nu(E,\hat{\mathbf{k}})\\&=\left(\frac{dR}{dE}\right)^{1/2}\left(\frac{dp}{dk}\right)^{-1/2}C_\nu(E,\hat{\mathbf{k}}).\end{aligned} \tag{3.7}$$

Substitution of these expressions in Eq. (3.3) gives the advanced adiabatic expression of Eq. (3.5).

The advanced adiabatic approximation derives from the Sturmian theory via the stationary phase approximation, and should be valid when there are points of stationary phase in the domain of integration. Alternatively, there may be no points of stationary phase in the allowed region. In that case the advanced adiabatic theory does not give the correct distribution.

For the u symmetry we find that $\mathrm{Im}\,p_\nu(k)<\mathrm{Re}\,p_\nu(k)$ so that there is a point of stationary phase in the allowed region. In this case Eq. (3.3) gives the advanced adiabatic result

$$\begin{aligned}|T_{\mathbf{k},i}^-|^2=&\frac{1}{\pi v k}\,\frac{Z_1}{\sqrt{k^2+Z_1^2}}\left|\frac{p_\nu(k)}{1-ip_\nu(k)}\sin^2\left[\frac{p_\nu(k)\cos\theta}{2}\right]\right|\\&\times\exp\left[-\frac{2}{v}\,\mathrm{Im}\int_0^k p_\nu(k')dk'\right].\end{aligned} \tag{3.8}$$

This expression is compared with the exact result at one angle in Fig. 3(a). The advanced adiabatic theory is indistinguishable from the exact distribution on this scale. On a finer scale (not shown) it is seen that the advanced adiabatic expression never deviates by more than 6% from the exact at $v=0.1$. Even for a higher velocity of $v=1.0$, the disagreement is never greater than 25%. We can conclude that the advanced adiabatic approximation gives a reliable *ab initio* electron distribution at low velocity in this model when the conditions for its validity are fulfilled.

Integrating over electron rejection angles gives the electron energy distribution. While this distribution is not needed for the results reported here, for completeness expressions for the energy distribution are given in Appendix C.

Alternatively, for g states we find $\mathrm{Im}\,p_\nu(k)>\mathrm{Re}\,p_\nu(k)$ and there is no point of stationary phase in the allowed region. In this case the advanced adiabatic approximation

$$\begin{aligned}|T_{\mathbf{k},i}^-|^2=&\frac{Z_1}{\pi v k}\,\frac{1}{\sqrt{k^2+Z_1^2}}\left|\frac{p_\nu(k)}{1-ip_\nu(k)}\cos 2\left[\frac{p_\nu(k)\cos\theta}{2}\right]\right|\\&\times\exp\left[-\frac{2}{v}\,\mathrm{Im}\int_0^k p_\nu(k')dk'\right]\end{aligned} \tag{3.9}$$

is expected to fail. The failure is verified in Fig. 3(b) where Eq. (3.9) and the exact results at $\theta=0$ are compared over an extended energy range. The distributions disagree by orders of magnitude except near $k=0$.

To obtain an expression valid when there is no point of stationary phase we approximate the Sturmian eigenvalue by an expansion around its first, generally complex, zero p_0;

$$\rho_\nu(p)\approx\alpha(p/p_0-1). \tag{3.10}$$

The function $F(k)$ is evaluated with this approximation in Appendix D. One has

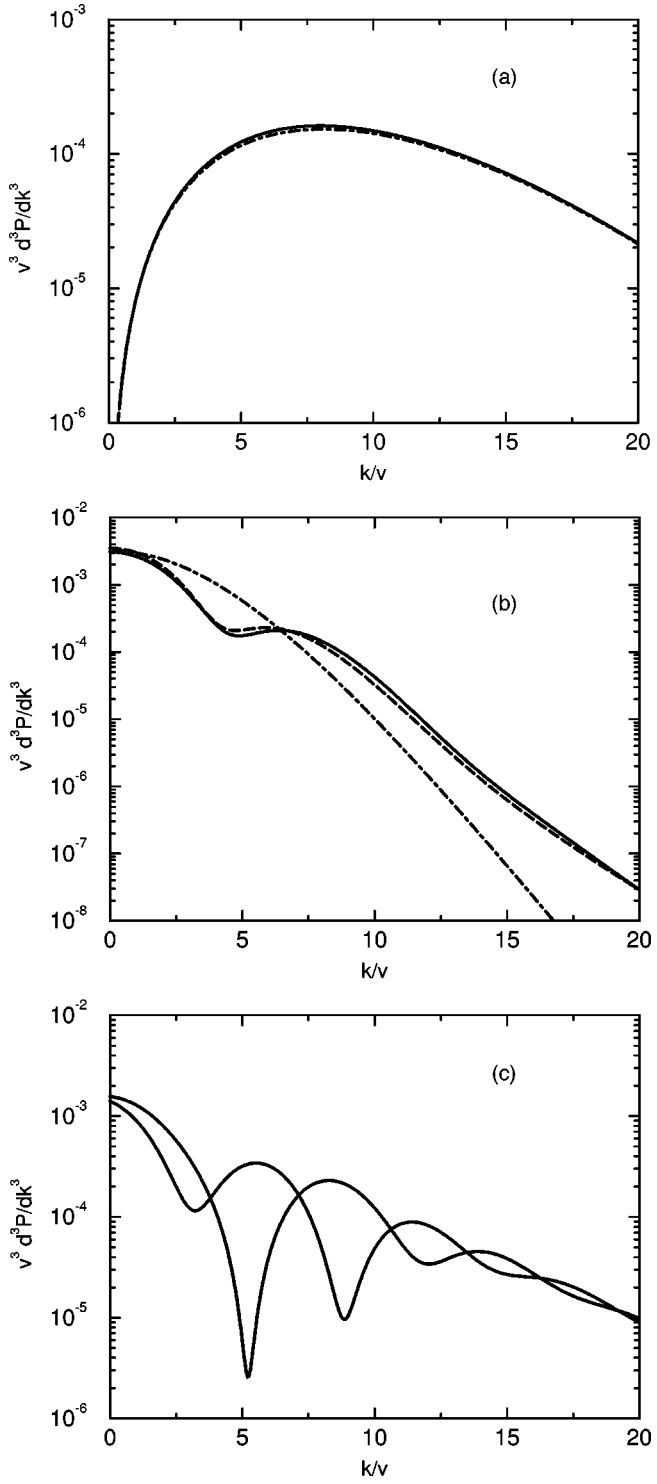

FIG. 3. Comparison of exact, solid curve, and advanced adiabatic, dot-dashed, distributions $v^3 d^3P/dk^3$ vs k/v for $\theta=0°$, $v=0.1$ a.u. in the center of mass frame. The curves for $v=0.1$ a.u. are indistinguishable on the scale for the u symmetry in (a) whereas the exact and advanced adiabatic distributions for the g symmetry in (b) differ by orders of magnitude except near $k=0$. The approximate Sturmian theory of Eq. (3.11), dashed curve, is seen to be in excellent agreement with the exact distribution over an extended electron momentum range. In (c), the distribution corresponding to an electron initially on the projectile is shown. Out of phase oscillations correspond to Fermi acceleration.

$$
\begin{aligned}
F(k) &= [I_1(k)+I_1(-k)]-[I_1^*(-k)+I_2(k)]T(0) \\
&\quad + i(\mathrm{Im}\, p_0/j)(p_0/p_0^*)[ikI_1(-k)+1], \\
T(0) &= -i(\mathrm{Im}\, p_0/p_0^*)e^{2j}(2j)^{-2j+1}\Gamma(2j-1,2j), \\
I_1(k) &= p_0(ikp_0+j)^{-j-1}\exp(ikp_0+j)\Gamma(j+1,ikp_0+j), \\
I_2(k) &= \Gamma^{-1}(2j-1,2j)\int_0^\infty dx(1+x/p_0)^j \\
&\quad \times \exp(jx/p_0-ikx)\Gamma(2j-1,2j+2jx/p_0),
\end{aligned}
\tag{3.11}
$$

where $\Gamma(a,x)$ is the incomplete gamma function [26], and $j=ip_0^2\alpha/v$.

The approximate Sturmian expression is found to be in good agreement with exact calculations for $v=0.1$, as shown by the dashed curve in Fig. 3(b). This emphasizes that the advanced adiabatic approximation fails for g symmetry owing to the lack of a stationary phase point $\rho(\omega)=R$ for physical values of R.

Electron velocities of $k\approx v=0.1$ a.u. correspond to electrons with an energy of 273 meV, which are too slow to be analyzed by conventional electron analyzers. For that reason interest attaches to the relatively fast electrons with $E_k \approx 0.5(10v)^2 \approx 13$ eV. In this case the approximate expression evaluated in Appendix E has the form

$$
F(k)=\frac{i8\alpha}{p_0 v}k^{-4}, \quad k\gg 1. \tag{3.12}
$$

It is important to note that the electron distribution falls off as a power of electron energy E_k, in this case as E_k^{-4}, rather than with the exponential decrease that obtains in the stationary phase approximation.

IV. DISCUSSION

Electron distributions for an exactly solvable model of atom–negative-ion collisions have been computed for both high and low ion velocities. The exactly solvable model uses zero-range potentials. Such potentials are commonly used to model negative-ion interactions in collisions, although low energy is usually emphasized. In this paper, the exact solutions have been expressed in terms of g and u Sturmian functions. Direct ionization cusps, continuum capture cusps, and the binary encounter ridge are identified at high velocity. These features are accurately modeled by expanding the exact transition amplitude in inverse powers of v, as is implicit in Born-type approximations for real collisions.

Distributions at low velocity exhibit Fermi acceleration peaks due to interference between g and u amplitudes. The u amplitudes are accurately calculated in the advanced adiabatic approximation, but the g amplitudes are not. An alternative approximate g amplitude was derived and found to agree well with the exact amplitude. The failure of the advanced adiabatic approximation for g symmetry was traced to a lack of a stationary phase point at physical values of R. Conversely, the success of this approximation for u symmetry was traced to the existence of a stationary phase point $\rho_-(\omega)=R$ at positive values of R.

The general Eq. (2.26) has also been interpreted in the hidden crossing sense. The exact expression *at all velocities* is given by an integral along some path in the complex R plane of an integrand involving only Demkov's general adiabatic function $\Phi(R;\mathbf{q})$, and eigenvalue $E(R)$. In this sense one sees that adiabatic functions can be used at all velocities, but they must be taken at complex R. The Sturmian theory provides a practical means to find the required complex values of R, namely, they are just the values of $\rho(\omega)$ for real ω.

The calculations presented here are based upon a single Sturmian function which is closely related to the complete set of adiabatic functions through Eq. (3.7). For real potentials there is a complete, and therefore infinite, set of Sturmian functions. Exact calculations employ a sufficient number of terms for the Sturmian expansion of $\chi(\omega,\mathbf{q})$ to converge. For the ZRP model presented here as well as the Demkov-Osherov [13] model, one Sturmian function [22], gives the exact solution. In the more general case, the one-Sturmian wave function is approximate, but the results presented here suggest that many qualitative features of the detached electron distributions emerge in the one-Sturmian approximation. In any event, application of the stationary phase approximation to the one-Sturmian wave function gives the advanced adiabatic approximation, which has been shown here to be quite reliable at low velocities provided the stationary phase conditions are met.

In summary, high- and low-velocity regions are connected through a single Sturmian function. Evaluating the amplitudes by expanding in inverse powers of v gives the high-velocity distribution, while evaluating them at low velocity in the stationary phase approximation gives the advanced adiabatic theory. When there is a point of stationary phase, the low-velocity distribution is quite reliable. This simple connection between high- and low-velocity regimes is the main contribution of the present manuscript.

ACKNOWLEDGMENTS

This research is sponsored by the Division of Chemical Sciences, Office of Basic Energy Sciences, U.S. Department of Energy, under Contract No. DE-AC05-96OR22464 through a grant to Oak Ridge National Laboratory, which is managed by Lockheed Martin Energy Research Corp. One of us (J.H.M.) gratefully acknowledges support by the National Science Foundation under NSF Grant No. PHY-9600017. This work was partly sponsored by a Macedonian-U.S. Joint Fund in cooperation with the National Science Foundation under Project Number 100.

APPENDIX A: TRANSITION AMPLITUDES FOR ZRPs IN THE STURMIAN REPRESENTATION

1. Transition amplitudes

Transition amplitudes to the continuum are given by [20]

$$T_{\mathbf{k},i}=\int \varphi_i^{\rm out}(\tau,\mathbf{q})\varphi_{\mathbf{k}}^{\rm in}(\tau,\mathbf{q})d^3\mathbf{q}$$
$$=\frac{i}{2\pi}\int_{-\infty}^{\infty}d\omega\int_{-\infty}^{\infty}d\omega' e^{-i(\omega-\omega')\tau}$$
$$\times\int \chi_i^{\rm out}(\omega',\mathbf{q})\chi_{\mathbf{k}}^{\rm in}(\omega,\mathbf{q})d^3\mathbf{q}. \tag{A1}$$

Substituting Eqs. (2.19) and (2.18) into Eq. (A1) gives the following expression for the transition amplitude:

$$T_{\mathbf{k},i}=\frac{i}{2\pi}\int_{-\infty}^{\infty}d\omega\, B_\nu^i(\omega)\int_{-\infty}^{\infty}d\omega'\, e^{-i(\omega-\omega')\tau}$$
$$\times\left[\frac{1}{\sqrt{2\pi}\nu^{3/2}}\int G_\nu^{\rm in}(\omega';\mathbf{k}/\nu,\mathbf{q})S_\nu^{\rm out}(\omega;\mathbf{q})d^3\mathbf{q}\right.$$
$$\left.+B_\nu^{\mathbf{k}}(\omega')\int S_\nu^{\rm in}(\omega';\mathbf{q})S_\nu^{\rm out}(\omega;\mathbf{q})d^3\mathbf{q}\right], \tag{A2}$$

where we have used $S^{\rm in}=(S^{\rm out})^*$ and $G^{\rm in}=(G^{\rm out})^*$. Taking into account that the matrix elements

$$\int S_\nu^*(\omega';\mathbf{q})S_\nu(\omega;\mathbf{q})d^3\mathbf{q}=-\frac{\rho_\nu^*(\omega')-\rho_\nu(\omega)}{\omega'-\omega}=\frac{R_{\nu\nu}(\omega)}{\omega'-\omega}, \tag{A3}$$
$$\int G_\nu^*(\omega';\mathbf{q},\mathbf{q}')S_\nu(\omega;\mathbf{q})d^3\mathbf{q}=\frac{S_\nu^*(\omega';\mathbf{q}')-S_\nu(\omega;\mathbf{q}')}{\omega'-\omega}$$
$$=\frac{R_\nu^{(G)}(\omega;\mathbf{q})}{\omega'-\omega}$$

have first order poles at $\omega=\omega'$ with residues $R_{\nu\nu}(\omega)$ and $R_\nu^{(G)}(\omega,\mathbf{q})$ gives

$$T_{\mathbf{k},i}=\int_0^{\infty}d\omega\, B_\nu^i(\omega)\left[\frac{1}{\sqrt{2\pi}\nu^{3/2}}R_\nu^{(G)}(\omega;\mathbf{k}/\nu)\right.$$
$$\left.+B_\nu^{\mathbf{k}}(\omega)R_{\nu\nu}(\omega)\right]. \tag{A4}$$

Substituting Eqs. (2.22), (2.23), and (A3) into Eq. (A4) we find

$$T_{\mathbf{k},i}=-\frac{1}{\sqrt{2\pi}\nu^{3/2}}\int_0^{\infty}d\omega\left\{S_\nu(\omega;\mathbf{k}/\nu)B_\nu^i(\omega)\left[\frac{\rho_\nu^*(\omega)}{\rho_\nu(\omega)}\right.\right.$$
$$\left.\left.+T_\nu(\omega)\right]-S_\nu^*(\omega;\mathbf{k}/\nu)[B_\nu^i(\omega)+T_\nu(0)B_\nu^{i*}(\omega)]\right\}, \tag{A5}$$

where

$$T_\nu(\omega)=-\frac{i}{\nu}\frac{1}{D_\nu^2(\omega)}\int_\omega^{\infty}\frac{\rho_\nu(\omega')-\rho_\nu^*(\omega')}{\rho_\nu^2(\omega')}D_\nu^2(\omega')d\omega'. \tag{A6}$$

Integrating by parts in Eq. (A5) gives Eq. (2.27) of Sec. II, namely,

$$T_{\mathbf{k},i}=\frac{i}{\sqrt{2\pi}\nu}\int_0^{\infty}d\omega\left\{\frac{\partial S_\nu(\omega;\mathbf{k}/\nu)}{\partial\omega}D_\nu(\omega)[1-T_\nu(\omega)]\right.$$
$$\left.-\frac{\partial S_\nu^*(\omega;\mathbf{k}/\nu)}{\partial\omega}[D_\nu(\omega)-T_\nu(0)D_\nu^*(\omega)]\right\}. \tag{A7}$$

It is convenient to introduce a new variable $p=\sqrt{2\omega}$ and rewrite Eq. (A7) in the form

$$T_{\mathbf{k},i}=\frac{i}{\sqrt{2\pi}v}\int_0^\infty dp\,\frac{\partial S_\nu(p^2/2;\mathbf{k}/v)}{\partial p}\times\exp\left[-\frac{y_\nu(p)}{v}\right]\{1-T_\nu(p)\}+\int_0^\infty dp\,\frac{\partial S_\nu^*(p^2/2;\mathbf{k}/v)}{\partial p}\times\left\{\exp\left[-\frac{y_\nu(p)}{v}\right]-T_\nu(0)\exp\left[-\frac{y_\nu^*(p)}{v}\right]\right\},\tag{A8}$$

where

$$y_\nu(p)=-i\int_0^p\frac{p'dp'}{\rho_\nu(p')},\tag{A9}$$

$$T_\nu(p)=-\frac{i}{v}\exp\left[\frac{2y_\nu(p)}{v}\right]\int_p^\infty dp'p'\frac{\rho_\nu(p')-\rho_\nu^*(p')}{\rho_\nu^2(p')}\times\exp\left[-\frac{2y_\nu(p')}{v}\right].\tag{A10}$$

2. Total ionization probability

The probability of recapture from the continuum is

$$P_{\rm rec}=|T_\nu(0)|^2,\tag{A11}$$

and is computed using

$$T_{i,i}=\int\varphi_i^{\rm out}(\tau,\mathbf{q})\varphi_i^{\rm in}(\tau,\mathbf{q})d^3\mathbf{q}=-\frac{i}{v}\int_0^\infty d\omega\,\frac{\rho_\nu(\omega)-\rho_\nu^*(\omega)}{\rho_\nu^2(\omega)}\,\frac{1}{D_\nu^2(\omega)}=T_\nu(0).\tag{A12}$$

The total ionization probability is

$$P_{\rm ion}=1-|T_\nu(0)|^2=2\,{\rm Re}\,Q_\nu(0)-[{\rm Im}\,Q_\nu(0)]^2,\tag{A13}$$

where

$$Q_\nu(p)=1-T_\nu(p)=-i\frac{2}{v}\exp\left[\frac{2y_\nu(p)}{v}\right]\int_p^\infty dp'p'\frac{{\rm Re}\,\rho_\nu(p')}{\rho_\nu^2(p')}\times\exp\left[-\frac{2y_\nu(p')}{v}\right].\tag{A14}$$

APPENDIX B: TRANSITION AMPLITUDES AT HIGH ENERGY

The spectrum of electrons for fast collisions contains two main features: cusps and binary encounter peaks. These features are determined by the behavior of Sturmian eigenvalues $\rho_\nu(p)$ at large $p\gg1$.

Sturmian eigenvalues in the limit $p\to\infty$ are given by

$$\rho_\nu(p)\sim-\frac{n}{Z_1}[ip+\beta_\nu(ip)^s\exp(ip)],\tag{B1}$$

where Z_1, n, and β are some constants. The corresponding potential energy curves in the limit $R\to\infty$ are [27]

$$E_\nu(R)\sim-\frac{Z_1^2}{2n^2}\left[1+2\beta\left(\frac{Z_1R}{n}\right)^{s-1}\exp\left(-\frac{Z_1R}{n}\right)\right].\tag{B2}$$

Equation (B1) is used in Eq. (2.32) written in the form

$$F_\nu(k)=\int_0^\infty\exp(ikp)\exp\left[-\frac{y_\nu(p)}{v}\right]Q_\nu(p)dp+\int_0^\infty\exp(-ikp)\left\{\exp\left[-\frac{y_\nu(p)}{v}\right]-\exp\left[-\frac{y_\nu^*(p)}{v}\right]\right\}dp+Q_\nu(0)\int_0^\infty\exp(-ikp)\exp\left[-\frac{y_\nu^*(p)}{v}\right]dp.\tag{B3}$$

Introducing the scaled velocity $\overline{v}=vn/Z_1$, a new function

$$x_\nu(p)=-\lim_{\epsilon\to0}\int_p^\infty\left(\frac{v}{\overline{v}}\frac{ip'}{\rho_\nu(p')}+1\right)\exp(-\epsilon p')dp',\tag{B4}$$

for which

$$y_\nu(p)=(v/\overline{v})[p-x_\nu(p)+x_\nu(0)],\tag{B5}$$

and using asymptotic expressions for $x_\nu(p)$ and $Q_\nu(p)$ as $p\to\infty$,

$$x_\nu(p)\sim-\beta p^{s-1}i^s\exp(ip),\qquad Q_\nu(p)\sim-i\frac{2\beta}{\overline{v}}p^{s-1}\,{\rm Re}\left[\frac{i^s\exp(ip)}{2/\overline{v}-i}\right],\tag{B6}$$

gives, for $s>0$, the result

$$F_\nu(k)\approx\frac{Q_\nu(0)\exp[-x_\nu^*(0)/\overline{v}]+2i\,{\rm Im}\{\exp[-x_\nu(0)/\overline{v}]\}}{1/\overline{v}+ik}+\frac{2\beta}{\overline{v}}\frac{d^{s-1}}{dk^{s-1}}\left\{\frac{{\rm Re}\{\exp[-x_\nu(0)/\overline{v}]\}}{1/\overline{v}+i(k+1)}+\frac{{\rm Re}\{\exp[-x_\nu(0)/\overline{v}]\}}{1/\overline{v}+i(k-1)}+\frac{\exp[-x_\nu(0)/\overline{v}]}{(1+i2/\overline{v})[1/\overline{v}-i(k+1)]}+\frac{\exp[-x_\nu(0)/\overline{v}]}{(1-i2/\overline{v})[1/\overline{v}-i(k-1)]}\right\}.\tag{B7}$$

For $s=0$, which corresponds to two 3D ZRPs, we find

$$F_\nu(k)\approx\frac{Q_\nu(0)\exp[-x_\nu^*(0)/\overline{\nu}]+2i\,\mathrm{Im}\{\exp[-x_\nu(0)/\overline{\nu}]\}}{1/\overline{\nu}+ik}$$
$$-i\frac{2\beta}{\overline{\nu}}\left\{\frac{\exp[-x_\nu(0)/\overline{\nu}]}{1+i2/\overline{\nu}}\left[\frac{1/\overline{\nu}+i(k^*+1)}{1/\overline{\nu}-i(k+1)}\right]^{1/2}\right.$$
$$-\frac{\exp[-x_\nu(0)/\overline{\nu}]}{1-i2/\overline{\nu}}\left[\frac{1/\overline{\nu}+i(k^*-1)}{1/\overline{\nu}-i(k-1)}\right]^{1/2}$$
$$+\mathrm{Re}\{\exp[-x_\nu(0)/\overline{\nu}]\}\left[\frac{1/\overline{\nu}-i(k^*+1)}{1/\overline{\nu}+i(k+1)}\right]^{1/2}$$
$$\left.-\mathrm{Re}\{\exp[-x_\nu(0)/\overline{\nu}]\}\left[\frac{1/\overline{\nu}-i(k^*-1)}{1/\overline{\nu}+i(k-1)}\right]^{1/2}\right\}. \quad \text{(B8)}$$

Equation (B8) shows that $F_\nu(k)$ has singularities at five points, namely, $k=-i/\overline{\nu}$ and $k=\pm1\pm i/\overline{\nu}$ for any $\overline{\nu}$. For fast collisions $\overline{\nu}\gg1$ we find

$$F_\nu(k)\approx\frac{2}{\overline{\nu}}\frac{z_\nu}{1/\overline{\nu}+ik}+\frac{2\beta_\nu}{\overline{\nu}^2}\left\{\frac{2-(k+1)[\mathrm{Im}\,x_\nu(0)-2]}{[(1/\overline{\nu})^2+(k+1)^2]^{1/2}}\right.$$
$$\left.-\frac{2-(k-1)[\mathrm{Im}\,x_\nu(0)+2]}{[(1/\overline{\nu})^2+(k-1)^2]^{1/2}}\right\}, \quad \text{(B9)}$$

where

$$z_\nu=\frac{Q(0)\nu}{2}-i\,\mathrm{Im}\,x_\nu(0)$$
$$=-\frac{2\nu}{\overline{\nu}}\lim_{\epsilon\to0}\int_0^\infty dp\,p\,\frac{\mathrm{Re}\,\rho_\nu(p)\mathrm{Im}\,\rho_\nu(p)}{\rho_\nu(p)|\rho_\nu^2(p)|}\exp(-\epsilon p). \quad \text{(B10)}$$

For two 3D ZRPs $\beta_\nu=\pm1$, $x^+(0)=-1.13-i0.13$, $z^+=0.65+i0.38$, and $x^-(0)=-i0.76$, $z^-=1.56-i0.52$. In the case of two 1D ZRPs we have $z_\nu=0$, since $x_\nu(0)=iQ_\nu(0)\overline{\nu}/2$, and there are no cusp electrons.

APPENDIX C: ENERGY DISTRIBUTIONS

The energy distribution is

$$P(E)=k\int|T_{\mathbf{k},i}|^2\,d\hat{\mathbf{k}}$$
$$=\frac{k}{\nu}\left|\frac{dp_\nu(k)}{dk}c_\nu^2(p_\nu(k))\right|$$
$$\times\exp\left[-\frac{2}{\nu}\mathrm{Im}\int_0^k p_\nu(k')dk'\right]$$
$$=\frac{k}{\nu}\left|\frac{dR_\nu(E)}{dE}C_\nu^2(E)\right|$$
$$\times\exp\left[-\frac{2}{\nu}\mathrm{Im}\int_0^E R(E')dE'\right], \quad \text{(C1)}$$

where

$$|C_\nu^2(E)|=\int|C_\nu(E,\hat{\mathbf{k}})|^2\,d\hat{\mathbf{k}},$$
$$|c_\nu^2(p_\nu(k))|=\int|c_\nu^2(p_\nu(k),\hat{\mathbf{k}})|^2\,d\hat{\mathbf{k}}. \quad \text{(C2)}$$

This result differs from Ref. [10] by the definition of $C(E)$. There $C(E)$ was incorrectly defined as $C_\nu(E)=\int C_\nu(E,\hat{\mathbf{k}})d\hat{\mathbf{k}}$. Usually $C(E)$ is not known, and an approximation based upon the Demkov-Osherov model is used. In that model [13,12] $S(E;\mathbf{r})=\sqrt{dR(E)/dE}\Phi_\nu(R(E);\mathbf{r})$ is a Sturmian function and $R_\nu(E)$ is a Sturmian eigenvalue, then $|C_\nu^2(E)|$ is found by comparing

$$\int S_\nu^*(E';\mathbf{q})S_\nu(E;\mathbf{q})d^3\mathbf{q}=-\frac{\rho_\nu^*(E')-\rho_\nu(E)}{E'-E} \quad \text{(C3)}$$

and

$$\int S_\nu^*(E';\mathbf{r})S_\nu(E;\mathbf{r})d^3\mathbf{r}\to\left[\frac{dR_\nu(E)}{dE}\right]\frac{\int|C_\nu(E,\hat{\mathbf{r}})|^2\,d\hat{\mathbf{r}}}{\sqrt{2E'}-\sqrt{2E}}$$
$$\text{as}\quad E'\to E. \quad \text{(C4)}$$

One finds

$$|C_\nu^2(E)|=\left[\frac{dR_\nu(E)}{dE}\right]^{-1}\frac{2\,\mathrm{Im}\,R_\nu(E)}{\sqrt{2E}}. \quad \text{(C5)}$$

In our theory, $S(E;\mathbf{r})$ is not a Sturmian function, rather $S(p,\mathbf{q})$ is, therefore, using the same arguments, we find

$$|c_\nu^2(p_\nu(k))|\approx\frac{\mathrm{Im}\,\rho_\nu(p(k))}{p(k)}=\frac{2\,\mathrm{Im}\,p(k)}{kp(k)},$$
$$\text{if}\quad \mathrm{Im}\,p(k)\ll\mathrm{Re}\,p(k). \quad \text{(C6)}$$

With this expression, we obtain

$$P(E)\approx\frac{2\,\mathrm{Im}\,p_\nu(k)}{\nu}\left|\frac{dp_\nu(k)}{dk}\frac{1}{p_\nu(k)}\right|$$
$$\times\exp\left[-\frac{2}{\nu}\mathrm{Im}\int_0^k p_\nu(k')dk'\right]$$
$$\approx\frac{2\,\mathrm{Im}\,R_\nu(E)}{\nu}\left|1+\frac{2E}{R_\nu(E)}\frac{dR_\nu(E)}{dE}\right|$$
$$\times\exp\left[-\frac{2}{\nu}\mathrm{Im}\int_0^E R(E')dE'\right]. \quad \text{(C7)}$$

Our result Eq. (C7) for $P(E)$ differs from Eq. (C5) by the second term inside the absolute value sign. In some regions of the spectrum the second term is significant and should be retained.

For the u state of two 3D ZRPs we find that $\mathrm{Re}\,p_\nu(k)>|\mathrm{Im}\,p_\nu(k)|>0$ for all $k>0$. Then the adiabatic expression

$$|T_{\mathbf{k},i}|^2=\frac{1}{\pi\nu k}\frac{Z_1}{\sqrt{k^2+Z_1^2}}\left|\frac{p_\nu(k)}{1-ip_\nu(k)}\sin^2\left[\frac{p_\nu(k)\cos\theta}{2}\right]\right|$$
$$\times\exp\left[-\frac{2}{\nu}\mathrm{Im}\int_0^k p_\nu(k')dk'\right] \quad \text{(C8)}$$

accurately describes the spectrum for $k>\nu$ and $\nu<1$.

The energy distribution, obtained by integrating over angles, is

$$P(E)=\frac{2}{\nu}\frac{Z_1}{\sqrt{k^2+Z_1^2}}\left|\frac{p_\nu(k)}{1-ip_\nu(k)}\left[\frac{\sinh(\mathrm{Im}\,p_\nu)}{\mathrm{Im}\,p_\nu}-\frac{\sin(\mathrm{Re}\,p_\nu)}{\mathrm{Re}\,p_\nu}\right]\right|\exp\left[-\frac{2}{\nu}\mathrm{Im}\int_0^k p_\nu(k')dk'\right]$$
$$\approx\frac{2}{\nu}\frac{Z_1}{\sqrt{k^2+Z_1^2}}\left|\frac{p_\nu^3(k)}{1-ip_\nu(k)}\left(1-\frac{\sin p_\nu}{p_\nu}\right)\right|\times\exp\left[-\frac{2}{\nu}\mathrm{Im}\int_0^k p_\nu(k')dk'\right]. \quad \text{(C9)}$$

For slow electrons $k\ll 1$ we can use the approximation $p_\nu(k)\approx k/Z_1$, then

$$P(E)\approx\frac{k^3}{3\nu Z_1^2}. \quad \text{(C10)}$$

For fast electrons $k\gg 1$, the alternative approximation,

$$p_\nu(k)\approx\frac{k}{Z_1+k/k_0^-}, \quad \text{(C11)}$$

where $k_0^-\approx 1.337+i0.318$ is determined from the equation $ik_0^-=\exp(ik_0^-)$, gives

$$\int_0^k p_\nu(k')dk'=k_0k-k_0^2Z_1\ln[1+k/(k_0^-Z_1)] \quad \text{(C12)}$$

and

$$P(E)\approx\frac{2Z_1}{\nu k}\left|\frac{k_0}{1-ik_0}\left(1-\frac{\sin k_0}{k_0}\right)\left(\frac{k_0Z_1}{k}\right)^{i2k_0^2Z_1/\nu}\right|\times\exp\left(-\frac{2}{\nu}\mathrm{Im}\,k_0k\right). \quad \text{(C13)}$$

APPENDIX D: TRANSITION AMPLITUDES AT LOW ENERGY

For g states we approximate the Sturmian eigenvalues $\rho_\nu(p)$ by an expansion around their first zero,

$$\rho_\nu(p)\approx\alpha(p/p_0-1), \quad \text{(D1)}$$

and obtain

$$T_{\mathbf{k},i}^{\pm}=\frac{1}{2\nu\pi\sqrt{Z}}\left[F^{\pm}\left(\left|\frac{\mathbf{k}}{\nu}+\frac{\hat{\mathbf{v}}}{2}\right|\right)\pm F^{\pm}\left(\left|\frac{\mathbf{k}}{\nu}-\frac{\hat{\mathbf{v}}}{2}\right|\right)\right], \quad \text{(D2)}$$

where

$$F(k)=[I_1(k)+I_1(-k)]-[I_1^*(-k)+I_2(k)]T(0)+i(\mathrm{Im}\,p_0/j)(p_0/p_0^*)[ikI_1(-k)+1],$$
$$T(0)=-i(\mathrm{Im}\,p_0/p_0^*)e^{2j}(2j)^{-2j+1}\Gamma(2j-1,2j),$$
$$I_1(k)=p_0(ikp_0+j)^{-j-1}\exp(ikp_0+j)\Gamma(j+1,ikp_0+j), \quad \text{(D3)}$$
$$I_2(k)=\Gamma^{-1}(2j-1,2j)\int_0^\infty dx(1+x/p_0)^{-j}\times\exp(jx/p_0+ikx)\Gamma(2j-1,2j+2jx/p_0),$$

with $j=ip_0^2\alpha/\nu$. For fast electrons $k\gg 1$ at all velocities we find

$$F(k)=\frac{i8\alpha}{p_0\nu}k^{-4}. \quad \text{(D4)}$$

For slow collisions $\nu\ll 1$ we also have

$$T(0)=-i\frac{\mathrm{Im}\,p_0}{2jp_0^*}\left(\sqrt{\frac{i\pi}{\nu}}p_0-\frac{4}{3}\right). \quad \text{(D5)}$$

APPENDIX E: FAST ELECTRONS

This part of the electron spectrum is determined by the behavior of Sturmian eigenvalue $\rho_\nu(p)$ at small $p\ll 1$. We will consider two cases, namely, $\rho_\nu(p)\to R_c\neq 0$ as $p\to 0$, associated with ionization via promotion to the continuum and $\rho_\nu(p)\to 0$ as $p\to 0$, associated with ionization via decoupling. In the case of promotion to the continuum we write Sturmian eigenvalues in the limit $p\to 0$ as

$$\rho_\nu(p)=R_c\left[1+\sum_{s=1}^{k+1}\alpha_sp^{2s}+i\beta p^{2k+1}\right]+O(p^{2k+3}), \quad \text{(E1)}$$

where R_c, α_s, and β are some constants. The corresponding potential energy curves have the form

$$E_\nu(R)=-\frac{1}{2R_c^3\alpha_1}\left[(R_c-R)+i\beta R_c\left(\frac{R_c-R}{\alpha_1R_c}\right)\right]+O(R_c-R)^{k+1} \quad \text{(E2)}$$

for $k\neq 0$ and

$$E_\nu(R)=-\frac{(R_c-R)^2}{2R_c^3\beta^2}+O(R_c-R)^3 \quad \text{(E3)}$$

for $k=0$. We obtain

$$F_\nu(k)\approx i\frac{8\beta(s+1)(2s+1)!}{R_c\nu k^{2s+4}}. \quad \text{(E4)}$$

For the g state of two 3D ZRPs we have $s=0$, $R_c=-Z/2$, and $\beta=2$ so that

$$T_{\mathbf{k},i}\approx\frac{32}{\pi Z^{3/2}\nu^2k^4}. \quad \text{(E5)}$$

For the u state of two 3D ZRPs we have $s=1$, $R_c=Z/2$, and $\beta=1/6$, thus Eq. (E4) gives

$$T_{\mathbf{k},i}\approx i\frac{(2s+4)F_\nu(k)}{2\nu\pi\sqrt{Z}k}\cos\vartheta=\frac{96}{\pi Z^{3/2}\nu^2k^7}\cos\vartheta. \quad \text{(E6)}$$

For decoupling we write Sturmian eigenvalues in the limit $p\to 0$ as

$$\rho_\nu(p)=-\frac{inp}{Z}\left[1+\sum_{s=1}^{k+1}\alpha_s(np)^{2s}+i\beta(np)^{2k+1}\right]+O(p^{2k+3}), \quad \text{(E7)}$$

where Z, n, α_s, and β are some constants. The corresponding potential energy curves in the limit $R\to 0$ have the form

$$E_\nu(R)=-\frac{Z^2}{2n^2}\left[1+\sum_{s=1}^{k+1}\alpha_s'(ZR)^{2s}+(-1)^k2\beta(ZR)^{2k+1}\right]+O(R^{2k+3}). \quad \text{(E8)}$$

We find

$$F_\nu(k)\approx i\frac{8\beta(s+1)(2s+1)!}{\nu^2k^{2s+4}} \quad \text{(E9)}$$

for $s>0$ and

$$F_\nu(k)\approx i\frac{8\beta}{\nu^2k^4}+\frac{8\beta^2}{\nu k^4} \quad \text{(E10)}$$

for $s=0$.

[1] J. S. Briggs and J. H. Macek, Adv. At., Mol., Opt. Phys. **28**, 1 (1991).
[2] M. E. Rudd and J. H. Macek, Case Stud. At. Phys. **3**, 47 (1972).
[3] D. S. Crothers and J. F. McCann, J. Phys. B **16**, 3229 (1983).
[4] J. N. Madsen and K. Taulbjerg, J. Phys. B **28**, 1251 (1995).
[5] U. Fano, Phys. Today **29** (9), 32 (1976).
[6] M. Pieksma and S. Y. Ovchinnikov, Comments At. Mol. Phys. **31**, 21 (1995).
[7] E. A. Solov'ev, Phys. Rev. A **42**, 1331 (1990).
[8] E. A. Solov'ev, Zh. Eksp. Teor. Fiz. **81**, 1681 (1981) [Sov. Phys. JETP **54**, 893 (1981)].
[9] M. Pieksma and S. Y. Ovchinnikov, J. Phys. B **27**, 4573 (1994).
[10] E. A. Solov'ev, Zh. Eksp. Teor. Fiz. **70**, 872 (1976) [Sov. Phys. JETP **43**, 453 (1976)]; Usp. Fiz. Nauk. **157**, 437 (1989) [Sov. Phys. Usp. **32**, 228 (1989)].
[11] S. Yu. Ovchinnikov and J. Macek, Phys. Rev. Lett. **80**, 2298 (1998).
[12] Yu. N. Demkov and I. V. Komarov, Zh. Eksp. Teor. Fiz. **50**, 286 (1966) [Sov. Phys. JETP **23**, 762 (1966)].
[13] Yu. N. Demkov and V. I. Osherov, Zh. Eksp. Teor. Fiz. **53**, 1589 (1967) [Sov. Phys. JETP **26**, 916 (1968)].
[14] C. D. Lin (private communication).
[15] E. A. Solov'ev, Teor. Mat. Fiz. **28**, 240 (1976) [Theor. Math. Phys. **28**, 757 (1976)].
[16] J. Burgdörfer, J. Wang, and A. Bárány, Phys. Rev. A **38**, 4919 (1988).
[17] M. Rakovic and E. A. Solov'ev, Phys. Rev. A **41**, 3635 (1990).
[18] J. Wang, J. Burgdörfer, and A. Bárány, Phys. Rev. A **43**, 4036 (1991).
[19] S. Yu. Ovchinnikov and J. Macek, Phys. Rev. Lett. **75**, 2474 (1995).
[20] S. Yu. Ovchinnikov, J. H. Macek, and D. B. Khrebtukov, Phys. Rev. A **55**, 3605 (1997).
[21] S. Yu. Ovchinnikov and J. Macek, Phys. Rev. A **55**, 3605 (1997).
[22] J. H. Macek and M. Cavagnero, Phys. Rev. A **58**, 348 (1998).
[23] E. A. Solov'ev and S. I. Vinitski, J. Phys. B **18**, L557 (1985).
[24] Yu. N. Demkov, in *Proceedings of Invited Talks of the Fifth International Conference on the Physics of Electronic and Atomic Collisions, Leningrad, 1967*, edited by I. P. Flaks and E. S. Solovyev (Joint Institute for Laboratory Astrophysics, Boulder, CO, 1968), p. 186.
[25] C. R. Garraboti and R. O. Barrachina, Phys. Rev. A **28**, 2792 (1983); R. O. Barrachina, J. Phys. B **23**, 3221 (1990).
[26] *Handbook of Mathematical Functions*, edited by M. Abramowitz and I. A. Stegun, Natl. Bur. Stand. Appl. Math. Ser. No. 55 (U.S. GPO, Washington, DC, 1964), pp. 260 ff.
[27] I. V. Komarov, L. I. Ponomarev, and S. Y. Slavyanov, *Spheroidal and Coulomb Spheroidal Functions* (Nauka, Moscow, 1976), p. 124.